Effect of the Hydrodynamic Bearing on Rotor/Stator Contact in a Ring-Type Ultrasonic Motor

Takashi Maeno*
Canon Inc., 3-30-2 Shimomaruko,
Ohta-ku, Tokyo 145, Japan

David B. Bogy
Computer Mechanics Laboratory
Department of Mechanical Engineering
University of California, Berkeley CA 94720

Abstract

A hybrid numerical analysis that includes the hydrodynamic bearing effect and elastic contact in a ring-type ultrasonic motor is presented. The two dimensional Reynolds equation is solved numerically by a finite difference algorithm. The rotor deformation is described by a one dimensional Green's function obtained by using a finite element elastic analysis code. The contact problem is solved by an iteration method so that the contact condition and the hydrodynamic bearing condition are satisfied simultaneously. The results show that the hydrodynamic bearing effect is significant for ultrasonic frequency contact of the rotor and stator. Surface roughness, contact area, and normal vibrating speed of the stator are important parameters in the hydrodynamic bearing.

1. Introduction

Ultrasonic motors have been of interest in industry because of their unique characteristics such as high torque, low speed, simple design, silence, and high precision controllability. Several types of ultrasonic motors have been proposed[1]-[4]. They can be divided into two groups according to their contact principles between the stator (vibrating body) and a rotor/slider (driven body) . One is a traveling wave type, in which the contact area between the stator and rotor/slider moves with the traveling wave excited in the stator. The two bodies are always in contact near the wave crests. The other is a standing wave type, in which the two bodies contact at the same area intermittently.

A ring-type motor developed by Canon Inc. for autofocus lenses[5],[6] employs the traveling wave (See Fig. 1) . The traveling wave is excited in the stator ring by disjoined conductor films on a piezoelectric ceramic bonded to the side of the stator opposite from the teeth. A flange shaped rotor spring contacts the stator's teeth at the crests of the stator's traveling waves. The rotor, which is pressed against the stator with a certain normal force, is driven by means of the friction force at the contact areas.

In order to understand the contact characteristics of the ultrasonic motor, various researchers have undertaken theoretical and experimental studies in recent years. Ueha and Kurosawa[7] were the first to analyze the rotor/stator interface. They introduced a linear spring model for the rotor normal deformation and used it to calculate the motor's performance. Maeno et al.[8] calculated the mechanical characteristics of the ring type ultrasonic motor by using the JNIKE3D FE code. The elastic contact of the rotor/stator, considering the shear deformation of bodies by using a static friction coefficient μ_s and a dynamic friction coefficient μ_d , was simulated. In the above studies, the dynamic friction coefficient μ_d needed in the numerical analysis to produce agreement with experiments was different from the experimentally measured one.

In this study, we introduce the hydrodynamic bearing effect into the contact between the rotor and stator in a ring type ultrasonic motor. In section two, a hybrid numerical analysis scheme for solving the elastic contact and the hydrodynamic bearing simultaneously is presented. In section three, the calculated results are shown. The hydrodynamic bearing effect, especially the squeeze effect, is found to be significant for ultrasonic frequency contact of the rotor and stator. Surface roughness, contact area, and normal vibrating speed of the stator are important parameters for the hydrodynamic bearing. The disagreement between the friction coefficient needed in the numerical analysis and the experimentally measured one in the previous study is explained.

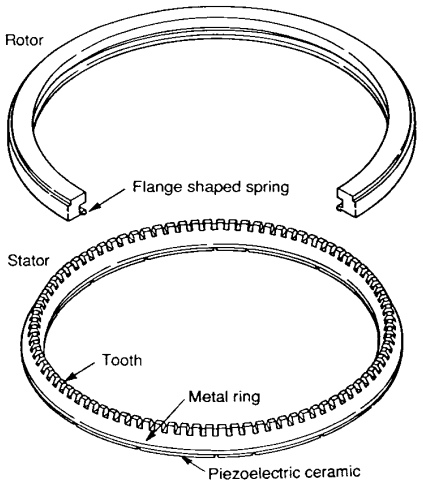

Figure 1 Ring-type ultrasonic motor

* : Visiting Industrial Fellow of the University of California, Berkeley

1051-0117/91/0000-0933 $1.00 © 1991 IEEE

2. Formulation

2-1 Reynolds Lubrication Equation

The first order compressible Reynolds lubrication equation for a finite width bearing, corrected for boundary slip, has the form,

$$\frac{\partial}{\partial x}\left[ph^3 \frac{\partial p}{\partial x}\left(1+\frac{6m}{ph}\right)\right] + \frac{\partial}{\partial y}\left[ph^3 \frac{\partial p}{\partial y}\left(1+\frac{6m}{ph}\right)\right] = \Delta \frac{\partial}{\partial x}[ph] + \Delta \frac{\partial}{\partial y}[ph] + \sigma \frac{\partial}{\partial t}[ph] \quad (1)$$

where, p(x,y,t) is the pressure, h(x,y,t) is the film thickness, Δ is the bearing number, σ is the so-called 'squeeze' number, and m is the Knudsen number, which relates the mean free path of the gas molecules to the minimum film thickness.

Linearizing equation (1) and introducing a rectangular mesh of p × q grid points within the bearing region, we can write the finite difference form of equation (1)[9] .

By solving the linear difference equation, we can obtain the pressure distribution p within the bearing region at the time step t from the given $p_{i,j}^{(t-\Delta t)}$, $h_{i,j}^{(t-\Delta t)}$, and $h_{i,j}^{(t)}$.

2-2 Stator vibration and rotor displacement

When the traveling wave is moving to the negative x-direction, the normal displacement of the stator at the top of the teeth, W_{Sn}, is,

$$W_{Sn}(i) = A_S \cos 2\pi \left(f t + \frac{\Delta x\,(i-1)}{\lambda} \right) \quad (2)$$

$$\Delta x = \frac{\lambda}{N}$$

where, A_S is the normal amplitude, f is the frequency, and λ is the wave length of the stator traveling wave. Also, N is the division number of the rotor in the circumferential direction through one wave length. On the other hand, the tangential displacement, W_{St}, is,

$$W_{St}(i) = B_S \sin 2\pi \left(f t + \frac{\Delta x\,(i-1)}{\lambda} \right) \quad (3)$$

where, B_S is the tangential amplitude. Also, the tangential velocity of the stator , V_{St}, is,

$$V_{St}(i) = \frac{\partial W_{St}}{\partial t} = 2\pi f B_S \cos 2\pi \left(f t + \frac{\Delta x\,(i-1)}{\lambda} \right) \quad (4)$$

We introduce a one dimensional Green's function for the rotor obtained by calculating the deformation of the actual three dimensional rotor corresponding to a normal point load using a FE code. If the discrete form of the Green's function is denoted by $G_{i,j}$, which represents the normal displacement of point j when a unit force is applied at point i, the normal displacement of the rotor at point j is,

$$W_R(j) = \sum_{i=1}^{N} G_{i,j} f_i \quad (5)$$

where, f_i is a point force applied at point i.

2-3 Hybrid analysis of the contact problem including the hydrodynamic bearing effect

A flow chart of the algorithm is shown in Fig. 2.

First, the displacement at the top of the stator teeth at time t due to the traveling wave is calculated by equation (2). Next, the rotor deformation is calculated by equation (5) so as to satisfy the assumed contact condition. For the initial calculation, the contact condition is assumed so that the positively displaced stator teeth contact the rotor. Then, the contact condition is checked to determine if the following equation is satisfied.

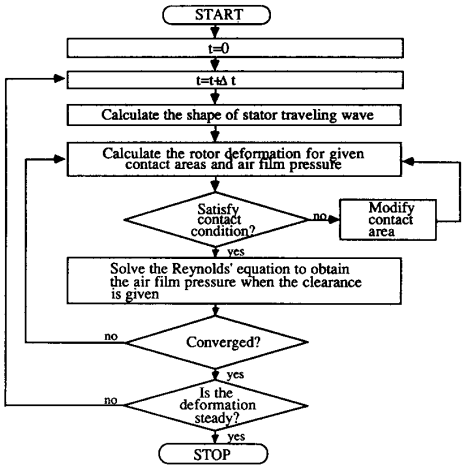

Figure 2 Flow chart of analysis

$$f_i > 0 \text{ and } W_R = W_{Sn} \text{ at contact grids,}$$
$$f_i = f_l \text{ and } W_R > W_{Sn} \text{ at noncontact grids} \quad (6)$$

If it is not satisfied, the contact condition is changed and the calculation of the rotor deformation is repeated. After the contact condition is satisfied, the hydrodynamic bearing pressure between each tooth and the rotor is calculated by the linearized Reynolds lubrication equation using the spacing at time t and t-Δt, the relative velocity at time t and t-Δt, and the pressure at time t-Δt. Since the pressure at t-Δt is not known for the initial calculation, the value zero is used for the initial pressure. Then the convergence condition is checked for the pressure and the spacing at time t. If convergence is not obtained, we go back to the calculation of the rotor deformation and repeat the above. If convergence is achieved, then we determine if the deformation and the pressure are steady, in another words, whether or not the deformation of the rotor and the pressure distribution are sufficiently near the previous cycle. The steady deformation and the pressure distribution are the required results of the solution.

In order to estimate the effect of the hydrodynamic bearing, we define a hydrodynamic bearing pressure ratio α by,

$$\alpha = \frac{\sum_{i=1}^{N} f_l(i)}{L} \quad (7)$$

$f_l(i)$: Hydrodynamic bearing load at node i

L : Total normal load

The ratio α indicates how much of the total load is provided by the hydrodynamic lubrication pressure. Since the friction coefficient of hydrodynamic lubrication μ_l is much smaller than μ_d ,

$$\mu_l \ll \mu_d$$

we can compute the maximum operating torque T_{max} by,

$$T_{max} = \mu_d (1-\alpha) L r \quad (8)$$

In this equation, a high α means a low maximum torque.

3 Calculated results

3-1 Fundamental case

The calculation is applied to various design parameters. At first, the deformation and the pressure are calculated for the actual rotor/stator geometry as shown in Fig. 3, which we call the "fundamental case". One wave length of the rotor is divided into 181 nodes. Each interface between a tooth and rotor is divided into 51 x 11 nodes as well.

Figure 4 shows the displacement of the rotor/stator and the pressure distribution of the fundamental case. The traveling wave moves to the left and the rotor moves to the right. The upper figure shows that the rotor contacts three stator teeth at this time. The lower figure shows that the hydrodynamic bearing effect on the rotor/stator contact is significant. Since the contact period is short, the hydrodynamic bearing pressure does not decrease while the rotor and stator contact. The hydrodynamic bearing pressure ratio α of the fundamental case is 0.24. (Hydrodynamic bearing pressure ratios for various design parameters are shown in table 1.) In order to explain the disagreement of the friction coefficient used in the calculation (μ_d=0.4) and the measured one (μ_d=0.7) in the previous study[8] , we need a hydrodynamic bearing pressure ratio of about 0.43. So the hydrodynamic bearing effect obtained is somewhat small for explaining the difference of μ quantitatively.

3-2 Effect of minimum spacing

The minimum spacing represents the mean clearance between the rotor and stator when they contact, in other words, a value proportional to the surface roughness. When the minimum spacing is 100 nm, ---- meaning that the surface roughness of the rotor and stator are about 100 nm p-p each ---- the hydrodynamic bearing pressure ratio α is up to 0.48. (See table 1) This result shows that the hydrodynamic bearing pressure increases when the minimum spacing decreases. In order to reduce the effect of the hydrodynamic bearing pressure, we must have a rough interface surface.

3-3 Effect of contact area

Results obtained for different teeth widths and rotor spring widths show that the resultant hydrodynamic bearing pressure is proportional to the interface area of the rotor/stator under the ultrasonic frequency vibration. (See table 1.) The smaller the interface area, the smaller the hydrodynamic bearing pressure ratio will be.

If the rotor stiffness is low, the contact area increases, and the hydrodynamic bearing pressure ratio α increases as well.

Table 1 Hydrodynamic bearing load and ratio α

Changed variables	Load(N)	Ratio
Fundamental case	0.583	0.238
p=101, q=21, N=361	0.595	0.243
Hm = 100 nm	1.179	0.481
Rotor width = 0.6 mm	1.141	0.466
Teeth width = 1.16 mm	0.386	0.157
Teeth width = 2.31 mm	0.779	0.318
Stator frequency = 3kHz	0.192	0.078
Stator frequency = 20kHz	0.550	0.224
Stator frequency = 40kHz	0.600	0.245
Stator frequency = 60kHz	0.615	0.251
Stator frequency =100kHz	0.630	0.257
Teeth radius = 3 m	0.576	0.235
Teeth radius = 6.5 m	0.585	0.239
Teeth radius = 10 m	0.586	0.239

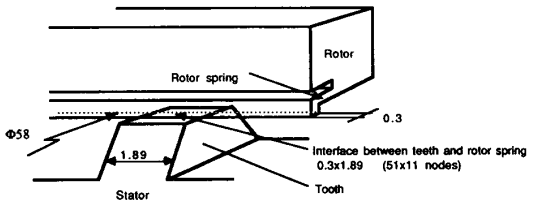

Contact diameter	58 mm
Traveling wave length	26 mm
Number of teeth per one traveling wave	9
Teeth width	1.89 mm
Rotor spring width	0.3 mm
Surface roughness	200 nm
Stator amplitude	2.0E-3 mmp-p
Rotor speed	180 mm/sec
Total load per one wave	2.45 N
Dynamic viscosity of air	0.181E-4 kg/m/sec
Atmospheric pressure	1.010E5 Pa
Mean free path of air	0.064E-6 m
Division of rotor on circumferential direction for contact analysis	181
Division of interface between stator and rotor spring	51x11

Figure 3 Schematic view of thr rotor/stator and the fundamental values used in the calculation

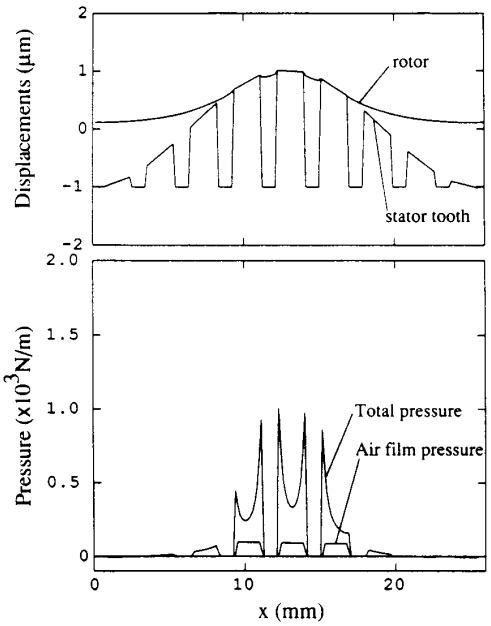

Figure 4 Normal displacement and pressure distribution (Fundamental case)

3-4 Effect of vibrating frequency

The effect of the stator vibrating frequency is studied by changing the stator frequency without changing the parameters, such as stator amplitude and rotor stiffness. Figure 5 shows the ratio α as a function of the vibrating frequency. When the frequency is higher, the normal velocity of the stator is higher and the squeeze effect is larger. If the frequency is changed without changing the rotational speed of the rotor, the change of normal velocity would be small, and the hydrodynamic bearing effect might be almost the same as for the fundamental case.

3-5 Effect of teeth geometry

The above calculation is performed by assuming that the rotor/stator surfaces are flat with sharp edges. But the actual macro geometry of a tooth surface is somewhat rounded at the edges and the pressure distributes more uniformly because of the wear, after it is driven for a few minutes. Therefore we made a calculation for curved teeth. When the arc radius is larger, the contact pressure distribution changes from the edge peaked shape to a half circle shape. When the radius of the teeth is 6.5 m, as shown in Fig. 6, the distribution of the contact pressure is almost uniform. Looking at the hydrodynamic bearing, we found that the distribution of the pressure and the ratio α scarcely change.

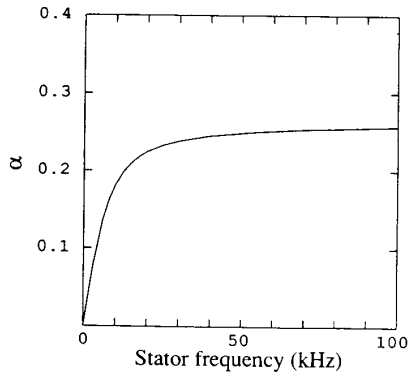

Figure 5 Effect of stator vibrating frequency

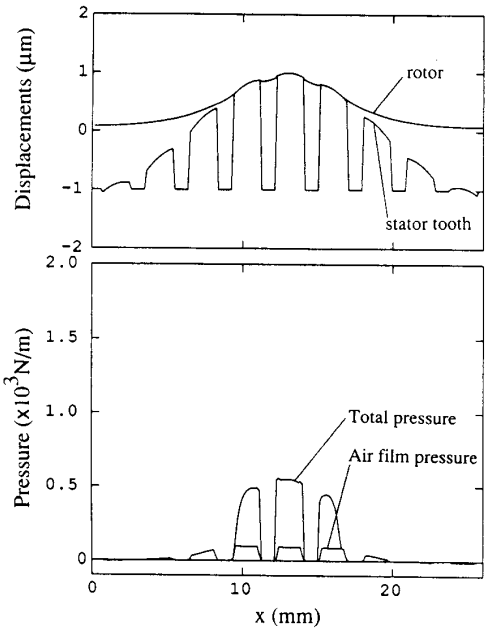

Figure 6 Normal displacement and pressure distribution (Teeth radius = 6.5 m)

4 Summary and discussions

A hybrid numerical analysis including the hydrodynamic bearing effect and elastic contact in a ring-type ultrasonic motor is completed. The calculation is applied to various design parameters and the results can be summarized as follows:

(1) Calculated results of the fundamental case show that the hydrodynamic bearing effect on the rotor/stator contact is significant.
(2) When the surface roughness of the rotor and stator decrease, the hydrodynamic bearing pressure ratio α increases. In order to reduce the effect of the hydrodynamic bearing pressure, we must increase the interface surface roughness.
(3) Results from changing the teeth width and the rotor spring width show that α is proportional to the interface area of the rotor/stator.
(4) When the frequency is higher, the normal velocity of the stator is higher and the ratio α is larger.
(5) When the arc radius of the teeth edges increases, the contact pressure distribution changes from the edge peaked shape to a half circle shape. On the other hand, the hydrodynamic bearing pressure distribution and the ratio α scarcely change.

References

[1] Sashida, T., "Ultrasonic Motor", Jpn. J. Appl. Phy., vol. 54-6, 1985, pp.589 (in Japanese)
[2] Ise, Y., "Ultrasonic Motor", J.Acoust.Soc.Jpn., vol. 54-6, 1985, pp.589 (in Japanese)
[3] Kumada, A., "A Piezoelectric Ultrasonic Motor", Jpn. J. Appl. Phy., vol. 24-2, 1985, pp.739
[4] Kurosawa, M. et. al., "An Ultrasonic Motor Using Bending Vibration of a Short Cylinder", IEEE Trans. UFFC, vol. 36, 1989, pp. 517
[5] Hosoe, K., "An Application of Ultrasonic Motor for Autofocus Lenses", Touhoku Univ. Tsuuken Symposium, 1989, pp. 117 (in Japanese)
[6] Okumura, I. and Mukohjima, H., "A Structure of Ultrasonic Motor for Autofocus Lenses", Proceeding Motor-Con '87, 1987, pp.75
[7] Kurosawa, M. and Ueha, S., "Efficiency of Ultrasonic Motor Using Traveling Wave", J.Acoust.Soc. Jpn., vol. 44-1, 1988, pp.40 (in Japanese)
[8] Maeno, T., Tsukimoto, T. and Miyake, A., "A Contact Mechanism of an Ultrasonic Motor", Proceeding ISAF '90, 1990
[9] White, J.W. and Nigam, A., "A Factored Implicit Scheme for the Numerical Solutions of the Reynolds Equation at Very Low Spacing", ASME J. of Lubr. Tech., vol. 102, No. 1, Jan. 1980, pp. 80-85
[10] Miu, D, "Dynamics of Gas-Lubricated Slider Bearings in Magnetic Recording Disk Files: Theory and Experiment", Dissertation, University of California, Berkeley, Dept. of Mechanical Engineering, 1985.
[11] Miu, D. and Bogy, D. B., "Dynamics of Gas-Lubricated Slider Bearings in Magnetic Recording Disk Files - Part II: Numerical Simulation", ASME J. of Tribology, vol. 108, 1986, pp. 589